Magneto-optics of nanoscale Bi:YIG films

Vladimir Berzhansky,[1] Tatyana Mikhailova,[1,*] Alexander Shaposhnikov,[1] Anatoly Prokopov,[1] Andrey Karavainikov,[1] Viacheslav Kotov,[2] Dmitry Balabanov,[3] and Vladimir Burkov[3]

[1]Taurida National V.I. Vernadsky University, 4 V.I. Vernadsky Avenue, Simferopol 95007, Ukraine

[2]V.A. Kotelnikov IRE RAS, 11 Mochovaya St., Moscow 125009, Russia

[3]Moscow Institute of Physics and Technology, 9 Institutskiy Lane, Dolgoprudny 141700, Russia

*Corresponding author: taciamikh@gmail.com

Received 12 June 2013; revised 7 August 2013; accepted 7 August 2013; posted 9 August 2013 (Doc. ID 192056); published 9 September 2013

Magnetic circular dichroism in the spectral region from 270 to 850 nm and Faraday rotation at the wavelength of 655 nm in ultrathin (1.5–92.8 nm) films prepared by reactive ion beam sputtering of target of nominal composition $Bi_{2.8}Y_{0.2}Fe_5O_{12}$ were studied. The observed effects of the "blue shift," inversion of the signs and change in the intensity of magneto-optical transitions, are discussed. It is demonstrated that all studied nanoscale films reveal magnetic properties—and their composition depends on the method of substrate surface pretreatment. © 2013 Optical Society of America

OCIS codes: (160.3820) Magneto-optical materials; (310.0310) Thin films; (230.2240) Faraday effect; (300.6170) Spectra; (020.3690) Line shapes and shifts.

http://dx.doi.org/10.1364/AO.52.006599

1. Introduction

In recent years, thin and ultrathin (less than 300 nm) highly bismuth-substituted yttrium iron garnet (Bi:YIG) films have been actively studied due to their role in device applications. For example, they are widely used in magneto-photonic crystal structures for magneto-optical (MO) devices [1–3]. Previous investigations [4–7] demonstrated that the properties of ultrathin films may significantly differ from the properties of thicker films. Sputtered ultrathin films frequently have high optical absorption and contain magnetically dead and/or passive interface and surface layers. These properties result from the presence of nanocrystalls forming magnetic layers and changing the composition of interfaces [6–9]. The films obtained by different methods of deposition have peculiarities. In addition, the methods of a substrate surface pretreatment affect the "surface morphology," optical and magneto-optical properties of the films [9]. This paper demonstrates that the influence of transition layers can be minimized and that the nanoscale highly Bi:YIG can be synthesized and used. The results of magnetic circular dichroism (MCD) and Faraday rotation (FR) measurements of ultrathin (1.5–92.8 nm) films, sputtered on pretreated $Gd_3Ga_5O_{12}$ (GGG) substrates by Ar^+ ions of different energy and current density, are discussed in relation to the existing models [4,10,11] for Bi:IG.

2. Experiment

The ultrathin Bi:YIG films were prepared by reactive ion beam sputtering (RIBS) of the target of nominal composition $Bi_{2.8}Y_{0.2}Fe_5O_{12}$ on (111) GGG substrates at room temperature in an argon–oxygen mixture. The substrates were pretreated before film deposition by either low-energy Ar^+ plasma (A films) or an Ar^+ ion beam with ion energy of 1 keV and current density of 2.5 $mA \cdot cm^{-2}$ (B films). The time of the ion pretreatment was 5 min for all substrates. The film thickness h was changed from 1.5 to 92.8 nm and

1559-128X/13/266599-08$15.00/0

calculated on the basis of the sputtering velocity of 5.8 nm per minute. The sputtered amorphous films were crystallized by annealing at a temperature of $T = 650$°C for 20 min [2,3,12].

The MCD effect was measured in the spectral region from 270 to 850 nm at magnetic field 5 kOe and in the temperature interval from 300 to 8 K by the Jobin–Yvon dichrograph model Mark IV. The MCD signal was determined as

$$A = [(I_+ - I_-)/(I_+ - I_-)]/h \ (\mathrm{cm}^{-1}), \tag{1}$$

where I_+ and I_- are the intensities of right and left circularly polarized light. The full thickness h of the film was used to calculate A without correction for the thickness of the sublayer nonmagnetic at room temperature.

FR or Faraday hysteresis loops (FHLs) were measured by the compensation method using a custom-made magneto-polarimeter at a wavelength of $\lambda = 655$ nm in the temperature region from 293 to 423 K. A custom-made magneto-polarimeter includes a light source (semiconductor laser), polarizer, MO modulator, electromagnet, compensator, analyzer, and photodetector. A special holder with a heater for temperature measurements, the sample, and a Hall sensor to measure the intensity of the magnetic field are placed in the gap of the electromagnet. The analyzer and polarizer are in the position of quenching of light. The compensator is a solenoid with diamagnetic glass (heavy flint) placed inside. The magnetic field changes in the range from −5 to 5 kOe. The signal from the photodetector is supplied to an electronic system and a personal computer with a control program for amplifying and processing.

Specific FR Θ_F, coercivity H_c, squareness coefficient K_s, saturation magnetic field H_s, Curie T_C, and compensation T_{comp} temperatures were determined from FHLs.

3. Magneto-Optical Relationships

MO effects in iron garnets (IGs) in geometry of experiment (the magnetization is parallel to the positive z direction) can be phenomenologically described by a dielectric tensor [11,13]

$$\hat{\varepsilon} = \begin{pmatrix} \varepsilon_{xx} & -i\varepsilon_{xy} & 0 \\ i\varepsilon_{xy} & \varepsilon_{xx} & 0 \\ 0 & 0 & \varepsilon_{zz} \end{pmatrix}, \tag{2}$$

where components ε_{xx} and ε_{xy} are complex, $\varepsilon_{xx} = \varepsilon'_{xx} + i\varepsilon''_{xx}$, and $\varepsilon_{xy} = \varepsilon'_{xy} + i\varepsilon''_{xy}$. The value of ε_{zz} is very close to ε_{xx} below T_C and is equal to ε_{xx} above T_C. ε_{xy} relates to specific FR Θ_F, MCD $\Delta\alpha$, refractive index n, and extinction coefficient k as

$$\varepsilon'_{xy} = -(\lambda/\pi)(n\Theta_F + k\Delta\alpha/4), \tag{3}$$

$$\varepsilon''_{xy} = -(\lambda/\pi)(\Theta_F k - n\Delta\alpha/4), \tag{4}$$

where λ is the wavelength of transmitted light.

In the region of the small absorption above $\lambda \sim 500$ nm for Bi:YIG, the following approximations are used:

$$\varepsilon'_{xy} = -\lambda n\Theta_F/\pi, \tag{5}$$

$$\varepsilon''_{xy} = \lambda n\Delta\alpha/4\pi. \tag{6}$$

For the shorter wavelength, the approximations are not as good but the qualitative relationships between the line shapes of ε'_{xy} and ε''_{xy} and measured spectra of Θ_F and $\Delta\alpha$ should still hold.

In the literature, the spectral variation of FR and the ellipticity (or MCD) in the visible and near-infrared ranges and off-diagonal permittivity tensor elements for Bi:YIG have been thoroughly investigated using both molecular-orbital analysis [4,10,11] and a charge-transfer transitions approach [10,11]. Current theories rely on the assumption that the substitution of Bi results in an overlap between the 6p orbital of Bi^{3+}, the 2p orbital of O^{2-}, and the 3d orbital of Fe^{3+}. This effect is quantum-mechanically described as a spin-orbit interaction that induces splitting in the energy levels of the corresponding orbitals. The most commonly used model is based only on electro-dipole diamagnetic type transitions and was developed by Wittekoek *et al.* [14], Dionne [11], and Helseth *et al.* [10,15]. Based on this model, Deb *et al.* [4] describe the MO properties of bismuth iron garnet (BIG) thin films in the spectral region between 295 and 730 nm as three diamagnetic type transitions with resonance wavelengths 299, 432, and 521 nm. The line shapes of these transitions also dominate in ε_{xy} spectra for Bi:YIG [10]. According to [11], two diamagnetic transitions above 350 nm relate to octahedral [a] and tetrahedral (d) sublattices and simultaneously participate in the iron-pair transitions. A transition at 299 nm presumably relates to the d sublattice [4,11]. As the magnetizations of a and d sublattices are opposite, a- and d-coordinated Fe^{3+} ions exhibit different signs of transitions. In the structure of Bi:YIG, $M_d > M_a$ and the d sublattice contributes the positive line shapes of ε_{xy} [11,13].

4. Results and Discussion

All MCD spectra of A and B films in the investigated range of thickness (at least for $h > 5.8$ nm) have the form that is typical for spectra of IG with high content of Bi: two peaks of opposite signs and the point of intersection with the wavelength axis (further "zero point," $A = 0$) [4,11,14]. The positions and amplitudes of short-wave (λ^i_{shw} and A^i_{shw}) and long-wave (λ^i_{lw} and A^i_{lw}) peaks as well as the value of wavelength λ^i_{zp} for the zero point depend on the resonant frequency, half width, and intensity (the density of active ions and oscillator strength) of MO transitions (i = A or B for A or B films, respectively) [11,13]. The MCD spectra for A and B films of thickness $h = 8.7$ nm measured at $T = 300$ K are shown in

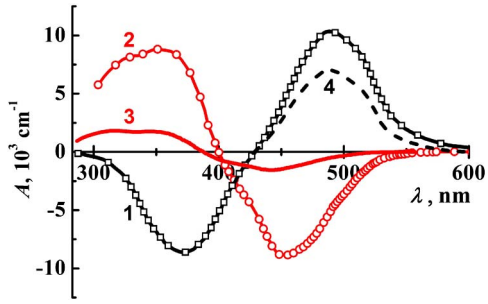

Fig. 1. MCD spectra for (1) 8.7 nm and (4) 5.8 nm A films and for (2) 8.7 nm and (3) 5.8 nm B films at 300 K.

Fig. 1 (lines 1 and 2). A^{A}_{lw} and A^{A}_{shw} of the spectrum of A film have the same signs as A_{lw} and A_{shw} of the MCD spectra of Bi:YIG ($A_{lw} > 0$ and $A_{shw} < 0$). In contrast, the spectrum of the B film is inverted ($A_{lw} < 0$ and $A_{shw} > 0$). This means that in a B film the orientation of sublattice magnetizations relative to the direction of the external magnetic field is opposite to the one found in Bi:YIG. The spectrum of B film is also shifted by an average of 30 nm in the "blue" region relative to the spectrum of A film. $|A^{B}_{shw}|$ slightly differs from $|A^{A}_{shw}|$, but $|A^{B}_{lw}|$ is less than $|A^{A}_{lw}|$ by 12%. In comparison to the spectrum of A film, B films exhibit broadening of the short-wavelength peak near 320 nm and a dip of the long-wavelength peak near 425 nm. This is typical for IG compounds with diamagnetic diluted d sublattice [11,15,16]. Presumably, the diamagnetic dilution leads to the reversal of the MCD spectrum of B film. As a result, the relative change of values and reorientation of magnetizations of a and d sublattices occur in the external magnetic field (so-called spin-reorientation transition from one ferrimagnetic (FIM) phase to another [17]).

Sixfold MCD intensity reduction, further "blue shift," and explicit dips in MCD peaks for spectra of 5.8 nm film (Fig. 1, line 3) indicate the increase of diamagnetic dilution that occurs with further decrease of the B-film thickness. The MCD amplitudes for A films of thicknesses 5.8, 2.9, and 1.5 nm are the same and account for 60% of the MCD signal of the thick films. However, a decrease of the A-film thickness results in the "blue shift" of spectra as well. The MCD spectra of 5.8 and 2.9 nm A films at 300 K are shown in Fig. 1 (line 4) and Fig. 2(a) (black solid line), respectively. MO activity at 300 K for a B film of thicknesses less than 5.8 nm is absent. In order to identify the MO properties, 2.9 nm B-film MCD spectra in the temperature range from 300 to 8 K were measured [Fig. 2(a)]. The weak MO activity occurs at $T \leq 250$ K. At temperatures from 250 to 150 K, the MCD signal is positive in all spectral regions besides the negative peaks near 500 and above 700 nm—and it is observed in the wide range of wavelengths. The spectra at these temperatures are not typical for Bi:YIG.

A spectral dependence with distinct peaks at wavelengths of 310, 340, 390, and 435 nm characteristic for MCD spectra of Bi:YIG [11,15,16] is observed at $T = 80$ K. At these low temperatures, the sign of MCD is inverted.

The temperature dependences of peak amplitudes A^{B}_{shw} and A^{B}_{lw} for 2.9 nm B film are shown in Fig. 2(b). The values of A^{B}_{shw} and A^{B}_{lw} at any temperature correspond to the values of MCD at $\lambda^{B}_{shw} = 305$ nm and $\lambda^{B}_{lw} = 392$ nm.

As temperature decreases, 2.9 nm B-film MCD spectra demonstrate magnetic phase transition from a paramagnetic (PM) phase to a FIM phase. According to MCD spectra [Fig. 2(a)], the Curie temperature T_C for 2.9 nm B film is approximately 130 K. Near and below this temperature, the magnetic order starts to form. A completely magnetic order is formed at $T = 80$ K. At temperatures from 250 to 130 K, where MCD signal is not zero, only a short-range magnetic order exists. The magnetic system splits into separate small clusters, and the MCD spectrum is shaped by individual contributions generated by these clusters. Similar temperature dependences of the magnetic order and the magnetizations in the vicinity of phase transition are typical for magnetics with thicknesses of several cell parameters, those with partial loss of translational invariance, and those significantly diluted by diamagnetic ions [18]. In comparison to 2.9 nm B film, 5.8 nm B film at temperatures from 300 to 8 K shows 2.3-fold increase of A_{lw} and a "blue shift" of 7 nm in the spectrum. A similar increase of MO effects with decreasing

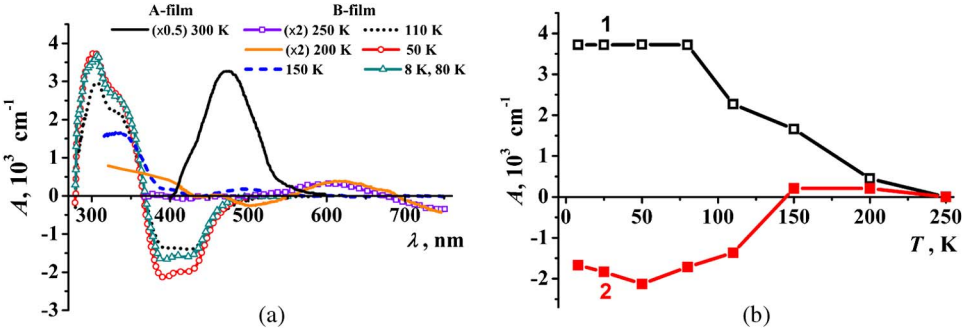

Fig. 2. (a) MCD spectra for 2.9 nm A film at temperature of 300 K and B film at different temperatures. The values of the MCD signal are twofold increased for B film at temperatures of 200 and 250 K and are halved for A film. (b) Peak amplitudes of MCD spectra versus temperature for 2.9 nm B film (1, short; 2, long-wavelength).

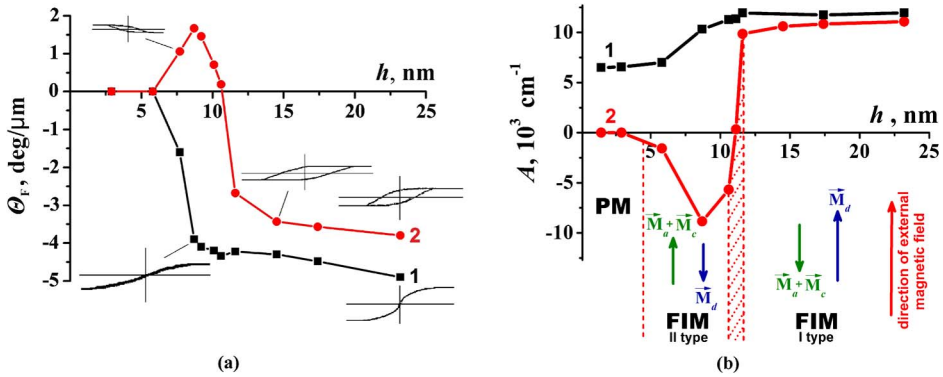

Fig. 3. Thickness dependences of (a) specific FR Θ_F and (b) MCD long-wave peak A_{lw} of ultrathin (1) A and (2) B films at saturated fields and temperature of 300 K. FHLs of the films at some thicknesses (not at equal scales) are shown in the insets of (a). (b) additionally shows observed magnetic phases for B films.

temperatures occurs in BIG films as well [19]. Changes in the refractive index, cell parameter, and magnetization affect the spectrum. In addition, with decreases of temperature to 8 K in 5.8 nm B film, the contribution to MO effects is provided by a layer that is more diamagnetic diluted and nonmagnetic at room temperature. This layer has a smaller lattice parameter and a weak exchange interaction. As a result, when the temperature decreases, the "blue shift" of the MCD spectrum is observed.

Figure 3 shows the changes in the intensity of MO effects [Fig. 3(a), specific FR Θ_F and FHLs; Fig. 3(b), MCD of long-wave peak amplitude A_{lw}] with increasing A- and B-film thicknesses from 1.5 to 23.2 nm and $T = 300$ K and the corresponding magnetic phase diagram for B films [Fig. 3(b)]. The sign of Θ_F at $\lambda = 655$ nm is opposite to the sign of A_{lw}, as it should be for the Bi:YIG [4,11,15,16].

The MO properties of A and B films thicker than 12 nm change slightly. Size effects (a significant change of MO and magnetic properties of films) are observed at thicknesses less than the critical $h_{\text{cr}} \approx 11$ nm. Dependences of $\Theta_F(h)$ and $A_{\text{lw}}(h)$ for B films are especially interesting due to the sign inversion in the vicinity of h_{cr} and a maximum at $h = 8.7$ nm. For B films, a weak MO activity at 300 K is present for 5.8 nm film (Fig. 1, line 3) and absent for films of thicknesses less than 5.8 nm. For the films of thicknesses less than 5.8 nm, the FR angle Θ_F becomes too small to measure within our detection limit. The phenomenon of the sign inversion of MO effects with the changes in B-film thickness was reproduced very well.

A films are characterized by "right" FHLs and in-plane or partly in-plane magnetic anisotropy in the whole region of thickness, as are conventional thick ($h \geq 100$ nm) Bi:YIG films. As A-film thickness decreases, a saturated field H_s increases 4–5 fold relative to the value measured in thick films—approaching 4.5 kOe for ultrathin films. B films have "left" FHLs and perpendicular anisotropy ($K_s =$ 0.8–0.9) at $h < h_{\text{cr}}$ and "right" FHLs at $h > h_{\text{cr}}$. The thickness dependence of H_C for B films has a maximum near $h_{\text{cr}} = 11$ nm (Fig. 4) that is characteristic of the temperature dependences of the coercive force in the vicinity of compensation temperature [17].

Thus, the results of MO measurements indicate that several phase transitions occur as the B-film thickness decreases [Fig. 3(b)]. The first phase transition from type-I FIM to type-II FIM, which is a manifestation of the compensation point in the external magnetic field [17], occurs in the vicinity of the critical thickness h_{cr} and depends on the external magnetic field and temperature of measurements. For sufficiently strong fields, this transition will be occurring through the intermediate spin-flop phase. At this point FIM appears as antiferromagnetic (this area is indicated by red dotted lines in Fig. 3). According to the measurements at different temperatures for B films with thicknesses close to h_{cr}, the orientation of sublattice magnetizations with respect to the external magnetic field is opposite at two temperature intervals: from 0 K to T_{comp} $M_a + M_c > M_d$ and from T_{comp} to T_{C} $M_{\text{a}} + M_c < M_d$. Here M_c is a magnetization of the dodecahedral $\{c\}$ sublattice due to substitution of Gd^{3+} ions. Films of thickness 11.1 and 9.7 nm have T_{comp} of 301 and 343 K, respectively. The B film of thickness 11.6 nm has T_{comp} at temperatures below room and $T_C \approx 393$ K. The films

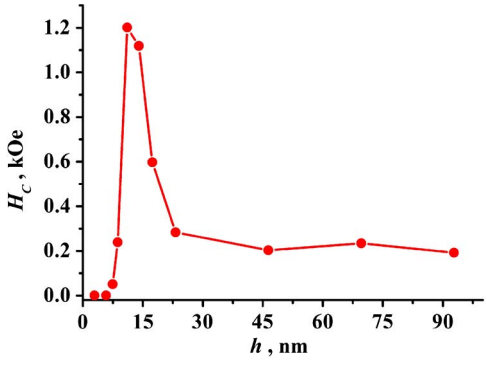

Fig. 4. Thickness dependence of H_C for B films at 300 K.

of composition $Bi_{2.8}Y_{0.2}Fe_5O_{12}$ must have $T_C \approx 630$ K [19]. As B-film thickness decreases, T_{comp} increases and exists for a certain range of film thicknesses; meanwhile, T_C decreases. As thickness drops to 5 nm, a second phase transition from the FIM phase to the PM phase occurs [Fig. 3(b)].

A films do not have the compensation temperature and have a single FIM phase; i.e., the orientation of sublattice magnetizations remains constant in the whole range of thicknesses.

A "blue shift" of MCD spectra as thickness decreases also strongly indicates the change of film composition. Figure 5 shows the position of characteristic points λ_{lw}, λ_{zp}, and λ_{shw} in MCD spectra as a function of thickness for A and B films. The "blue shift" of the spectra is observed for both A and B films with thicknesses below 15 nm [Fig. 5(b)]. The most significant changes occur in the spectrum of B films. The maximum values of the "blue shift" of characteristic points are $\delta^B_{lw} = 48$ nm, $\delta^B_{zp} = 27$ nm, and $\delta^B_{shw} = 13$ nm for B films and $\delta^A_{lw} = 4$ nm, $\delta^A_{zp} = 10$ nm, and $\delta^A_{shw} = 1$ nm for A films. For comparison, Table 1 shows the positions of characteristic points determined either from spectra of MCD (FR ellipticity) or elements of tensor ε_{xy} for Bi:IG of different compositions. In Fig. 5(b), the positions of characteristic points for compound Nos. 5, 14, and 6 from Table 1 are also shown by horizontal lines.

As one can see, the changes in the content of Fe^{3+} and Bi^{3+} ions identically and significantly change the λ_{lw}, but differently affect λ_{shw}. As the content of Bi^{3+} ions decreases, all characteristic points shift equally. In the case of dilution of Gd, Ga, and Al (Table 1, film No. 6), λ_{lw} experiences strong "blue shift" and λ_{shw} almost remains unchanged.

Both a decrease of B-film thickness in our experiments and a decrease of Bi and/or Fe content in other films of different composition in general lead to the same result: "blue shift" of MO transitions. Therefore, Bi and Fe contents decrease too while B-film thickness decreases from 23.2 to 1.5 nm. Positions of characteristic points λ^A_{lw}, λ^A_{zp}, and λ^A_{shw} of MCD spectra of A films vary slightly. According to x-ray diffraction patterns [9], the composition of 100 nm A film and, consequently, the A film with thickness of 10 nm is close to a target one ($a = 1.2602$ nm).

Both "blue shift" and decreases in the intensity of MO effects (Fig. 3) can be explained by the nature of MO transitions. First, the change of local crystal fields affecting octahedral and tetrahedral Fe^{3+} ions influences transition frequency [11,13]. Therefore, the lattice parameter and geometry of interatomic bonds affect λ_{lw}, λ_{zp}, and λ_{shw}. The lattice parameter is reduced faster with decreases in Bi content and slower with increases in Ga content. Similarly, the distortion of octahedra and tetrahedra leads to a change in transition frequencies. Second, those MO transitions in Fe^{3+} ions induced by Bi give the largest contribution to the spectrum and participate in the transitions between a- and d-coordinated Fe^{3+} ions. The content of Fe^{3+} and Bi^{3+} ions affects the energy of correlation intersublattice exchange and the number of magnetically intersublattice links (links with an admixture of Bi states) [11] that define the number of MO active Fe^{3+} ions. In addition, diamagnetic dilution leads to the appearance of local noncollinear spins [18] and difficulty of the intersublattice charge transfer that results in an increase of the energy of MO transitions.

The sharp "red shift" of the characteristic points for B films at h_{cr} [Fig. 5(b)] is caused by the observed compensation point. At this point, MO effects are created by Fe^{3+} ions that are linked by the strongest exchange interactions and have the maximum number of neighbors of Bi and Fe. These small parts of films have a greater lattice parameter. Unequal shifts of λ_{lw} and λ_{shw} with substitution of Bi by Gd and Fe by Ga are caused by different changes of energy, by half-linewidths, and by splitting parameters of MO transitions. As a consequence, these two cases demonstrate different contributions of the line shapes of MO transitions to the spectrum.

Insignificant dilution of diamagnetic ions is also present for A films of thickness less than 10 nm.

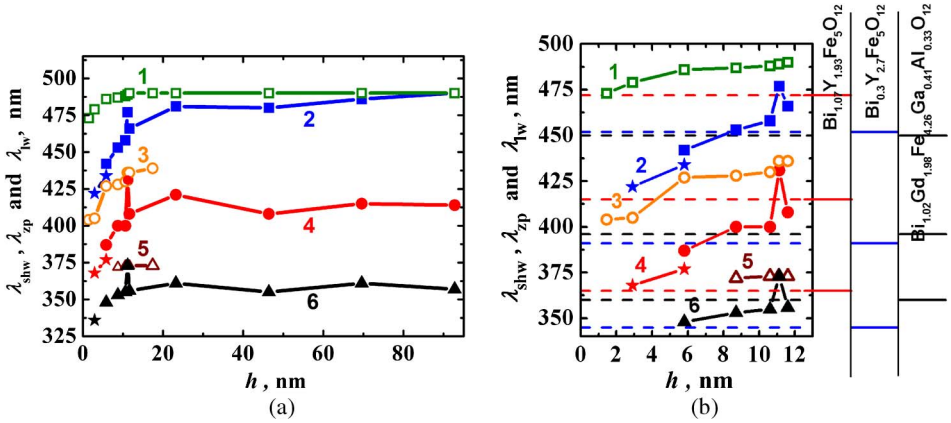

Fig. 5. "Blue shift" of positions of long-wave peaks (1) λ^A_{lw} and (2) λ^B_{lw}, short-wave peaks (5) λ^A_{shw} and (6) λ^B_{shw}, and zero points (3) λ^A_{zp} and (4) λ^B_{zp} with decreasing thickness for A and B films, respectively, at 300 K. Filled stars: corresponding positions for 5.8 and 2.9 nm B films at 8 K.

However, the growth of structural disorder and elastic stresses that change the crystalline electric fields is the main cause of the "blue shift" when film thickness decreases to less than 5 nm. The significant increase of H_s indicates the elastic stress increases.

It should be noted that the sputtering method and crystallization process of garnet films with high Bi content significantly affect MO properties. According to atomic force microscopy investigations [9], the crystallites' size in A films is greater than in B films. As the thickness of B films increases, the crystallite size increases as well. So, the difference between λ_{lw}, λ_{zp}, and λ_{shw} for A and B films and films with the same Bi^{3+} and Fe^{3+} ion content (Table 1), obtained by different methods, can be explained by the difference in the local crystal fields of a- and d-coordinated Fe^{3+} ions. The last is caused by the different formation of A and B films [9] and different geometry of interatomic bonds [21].

Similar reasoning may provide explanation of the above results for A and B films. In [22,23] it was shown that ion bombardment of the garnet sample (substrates bulk or film) damages its surface. Bombardment-induced bond angle disorder of the surface is associated with preferential resputtering of oxygen.

The effect of ion pretreatment of a GGG surface for A films is considerably smaller than for B films owing to the smallness of the energy and ion current density. The damaged amorphous layer in this case is less than 1 nm in depth [22].

The pretreatment of the GGG substrate surface by Ar^+ ions of 1 keV energy (B films) leads to the formation of a damaged amorphous layer on the GGG surface that is several nanometers in depth [23]. This layer may contain Ga and Gd oxides. During the crystallization annealing the solid phase reaction occurs in the bulk of this layer and the garnet phase containing Ga, Gd, Y, Bi, and Fe is formed. Due to the fact that in the initial amorphous film the substrate and the film elements in transition layers are distributed unevenly, the garnet films of composition $(BiGdY)_3(FeGa)_5O_{12}$ will have variable element contents across the film thickness during the crystallization process. A decrease of the film thickness leads to an increase in the volume fraction of the surface damaged layer of the GGG substrate and an increase in the content of Ga and Gd in the general film composition. Therefore, in the vicinity of critical thickness h_{cr} the concentrational spin-orientational phase transition occurs and Θ_F, A^B_{lw}, H_C and λ^i_{lw}, λ^i_{shw}, λ^i_{zp}, respectively, change (Figs. 1–5).

Despite the fact that films consist of nanocrystallites of different composition, the B film of thickness near $h_{cr} = 11$ nm behaves as a uniform film of composition $(BiGdY)_3Fe_{3.7}Ga_{1.3}O_{12}$. For the film $A = 0$ in the all-spectral range [Fig. 3(b)], T_{comp} is close to room temperature, H_C is maximal (Fig. 4), and $M_a + M_c = M_d$. At this concentration, Ga^{3+} replaces mainly d-coordinated Fe^{3+} ions and the fraction of d-coordinated Fe^{3+} ions is $k_d \approx 0.9$ [18]. The content of Ga^{3+} does not exceed 1 at./f.u.

The B film of thickness 8.7 nm, characterized by the maximum value of Θ_F and opposite signs of A (Fig. 3), behaves as a uniform film of composition $(BiGdY)_3Fe_{3.3}Ga_{1.7}O_{12}$. With increases in Ga content from 1.3 to 1.7 at./f.u. in the general composition of film, the absolute values of Θ_F and A increase due to corresponding augmentation of total magnetization and change of T_{comp} (the measurements were made at a temperature 300 K that is lower than T_{comp}). A further increase of Ga in the films with $h < 8.7$ nm leads to a change of the Fe fraction in sublattices ($k_d \leq 0.8$), a significant decrease of intersublattice links, and, as a consequence, total magnetization, T_C, Θ_F, and A. According to this, the B films with thickness of several cell parameters are greatly substituted by Ga ions (about 2 at./f.u.).

As Ga is distributed unevenly across the thickness of thick B films, the compensation plane must exist where the composition of the film is

Table 1. Position of Characteristic Points for Bi-Substituted IGs of Different Compositions

Nos.	Composition	Position of Characteristic Points			Synthesis Method	References
		λ_{lw}	λ_{zp}	λ_{shw}		
1	**$Bi_3Fe_5O_{12}$**	496	413	369	PLD	[4]
2	**$Bi_{2.8}Y_{0.2}Fe_5O_{12}$**[a](A films, $h > 24$ nm)	490	436	373	RIBS	This work
3	**$Bi_{2.8}Y_{0.2}Fe_5O_{12}$**[a](B films, $h > 24$ nm)	486	415	360	RIBS	This work
4	$Bi_1Gd_{1.5}Y_{0.5}Fe_{4.2}Al_{0.8}O_{12}$	469	413	359	RIBS	[8,9]
5	**$Bi_{1.07}Y_{1.93}Fe_5O_{12}$**	472	415	365	LPE	[16]
6	$Bi_{1.02}Gd_{1.98}Fe_{4.26}Ga_{0.41}Al_{0.33}O_{12}$	450	396	360	LPE	[16]
7	**$Bi_{0.5}LU_{2.5}Fe_5O_{12}$**	468	401	356	LPE	[15]
8	$Bi_{0.7}Lu_{2.3}Fe_{4.7}Ga_{0.3}O_{12}$	461	381	352	LPE	[15]
9	$Bi_{0.7}Lu_{2.3}Fe_{4.4}Ga_{0.6}O_{12}$	454	372	347	LPE	[15]
10	$Bi_{0.5}Tm_{2.5}Fe_{3.9}Ga_{1.1}O_{12}$	450	383	320	LPE	[13]
11	**$Bi_{0.47}Y_{2.53}Fe_5O_{12}$**	456	399	358	—	[11]
12	$Bi_{0.48}Y_{2.53}Fe_{4.5}Al_{0.5}O_{12}$	449	391	356	—	[11]
13	$Bi_{0.3}Pb_{01}Sm_{0.7}Gd_{0.2}Lu_{1.7}Fe_{4.3}Al_{0.5}Sc_{0.2}O_{12}$	447	400	350	LPE	[20]
14	**$Bi_{0.3}Y_{2.7}Fe_5O_{12}$**	452	391	345	LPE	[14]

[a]Indicates the nominal composition of the film (target composition). Unsubstituted by nonmagnetic ions (Ga, Al, etc.), compounds with different concentrations of Bi are bold. PLD, pulsed laser deposition; LPE, liquid phase epitaxy.

$(BiGdY)_3Fe_{3.7}Ga_{1.3}O_{12}$. The compensation plane is located at a distance 8.7 nm from the substrate as $\Theta_F(h)$ and $A(h)$ have maxima (Fig. 2). The fast drop in Ga and Gd content is expected in the thickness region higher than 8.7 nm. Presumably, the volume composition of B film in the thickness region higher than 12 nm is $Bi_{2.8}Y_{0.2}Fe_5O_{12}$. The gradient distribution of the elements is confirmed by our experiments on double-layer nanostructures [24].

It should be noted that MCD spectra in the region of strong magnetic ordering for all films are typical for the compounds with large number of Bi (Bi > 2 at. per f.u.). This conclusion is also supported by a higher T_C for Bi, Gd, and Ga:YIG than for Ga:YIG [13,18].

5. Conclusion

The MO properties of sputtered ultrathin (1.5–92.8 nm) bismuth-substituted IG films prepared by RIBS of target of nominal composition $Bi_{2.8}Y_{0.2}Fe_5O_{12}$ were studied. The substrates of GGG before film deposition were pretreated by either low-energy Ar^+ plasma (A films) or an Ar^+ ion beam with energy of 1 keV (B films).

In the case of B films, the substrate surface pretreatment leads to the substrate surface destruction and amorphization. As the film thickness decreases (below 15 nm), MCD spectra of B films demonstrate features of Ga and Gd dilution: the "blue shift" and change in intensity of MO transitions. MCD and FR measurements at 300 K show that as B-film thickness decreases, a series of magnetic phase transitions appears. Inversion of signs observed at the critical thickness of $h_{cr} = 11$ nm suggests a concentrational spin-orientation phase transition. According to MCD spectra measurements at different temperature for 2.9 nm B films, both long-range magnetic order and MCD spectra typical for IG are formed at temperatures less than 130 K. As a result, when thickness approaches 5 nm, the second phase transition from the FIM phase to the PM phase occurs. The distribution of Ga is not uniform along the film thickness, and the thickness of the film-substrate transition layer of B films is 15 nm.

The influence of the substrate surface pretreatment on the properties of A films is much less pronounced. MO activity at 300 K is present through all thickness ranges, even for the films of thickness 1.5 and 2.9 nm. Inverse effects are absent and "blue shift" is negligible. However, decreases of the intensity of MO transitions are still observed at thicknesses less than $h_{cr} = 11$ nm.

This work was supported by the Ministry of Education and Science of Ukraine and the State Fund for Fundamental Research of Ukraine.

References

1. M. Inoue, R. Fujikawa, A. Baryshev, A. Khanikaev, P. B. Lim, H. Uchida, O. Aktsipetrov, A. Fedyanin, T. Murzina, and A. Granovsky, "Magnetophotonic crystals," J. Phys. Appl. Phys. **39**, R151–R161 (2006).
2. V. N. Berzhansky, A. N. Shaposhnikov, A. R. Prokopov, A. V. Karavainikov, T. V. Mikhailova, E. Y. Semuk, M. I. Sharipova, T. V. Dolgova, A. A. Fedyanin, V. A. Kotov, and V. O. Golub, "One-dimensional magnetophotonic crystals based on double-layer Bi-substituted iron garnet films," Materialwiss. Werkstofftech **42**, 19–23 (2011).
3. V. N. Berzhansky, T. V. Mikhailova, A. V. Karavainikov, A. R. Prokopov, A. N. Shaposhnikov, I. N. Lukienko, Yu. N. Kharchenko, O. V. Miloslavskaya, and N. F. Kharchenko, "Microcavity one-dimensional magnetophotonic crystals with double layer iron garnet," J. Magn. Soc. Jpn. **36**, 42–45 (2012).
4. M. Deb, E. Popova, A. Fouchet, and N. Keller, "Magneto-optical Faraday spectroscopy of completely bismuth-substituted $Bi_3Fe_5O_{12}$ garnet thin films," J. Phys. Appl. Phys. **45**, 455001 (2012).
5. M. Veis, E. Lišková, R. Antoš, Š. Višňovský, N. Kumar, D. S. Misra, N. Venkataramani, S. Prasad, and R. Krishnan, "Polar and longitudinal magneto-optical spectroscopy of bismuth substituted yttrium iron garnet films grown by pulsed laser deposition," Thin Solid Films **519**, 8041–8046 (2011).
6. E. Popova, N. Keller, F. Gendron, L. Thomas, M.-C. Brianso, M. Guyot, M. Tessier, and S. S. P. Parkin, "Perpendicular magnetic anisotropy in ultrathin yttrium iron garnet films prepared by pulsed laser deposition technique," J. Vac. Sci. Technol. A **19**, 2567–2570 (2001).
7. E. Popova, N. Keller, F. Jomard, L. Thomas, M.-C. Brianso, F. Gendron, M. Guyot, and M. Tessier, "Exchange coupling in ultrathin epitaxial yttrium iron garnet films," Eur. Phys. J. B **31**, 69–74 (2003).
8. A. N. Shaposhnikov, A. R. Prokopov, A. V. Karavainikov, V. N. Berzhansky, I. V. Sharay, and V. G. Bar'yakhtar, "Bi-YIG films properties modifications by substrate surface ion pretreatment," in *Abstracts of International Conference On "Functional Materials" (ICFM-2011)* (DIP, 2011), p. 178.
9. A. N. Shaposhnikov, A. R. Prokopov, A. V. Karavainikov, V. N. Berzhansky, and T. V. Mikhailova, Taurida National V.I Vernadsky University, 4 V.I Vernadsky Avenue, Simferopol 95007, Ukraine, and V. A. Kotov, D. E. Balabanov, I. V. Sharay, O. Y. Salyuk, M. Vasiliev, and V. O. Golub are preparing a manuscript to be called "Modification of Bi:YIG film properties by substrate surface ion pre-treatment."
10. L. E. Helseth, R. W. Hansen, E. I. Il'yashenko, M. Baziljevich, and T. H. Johansen, "Faraday rotation spectra of bismuth-substituted ferrite garnet films with in-plane magnetization," Phys. Rev. B **64**, 174406 (2001).
11. G. F. Dionne, "Magneto-optical spectra," in *Magnetic Oxides* (Springer, 2009), pp. 355–382.
12. V. N. Berzhansky, A. V. Karavainikov, E. T. Milyukova, T. V. Mikhailova, A. R. Prokopov, and A. N. Shaposhnikov, "Synthesis and properties of substituted ferrite-garnet films for one-dimensional magnetophotonic crystals," Functional Materials **17**, 120–126 (2010).
13. A. K. Zvezdin and V. A. Kotov, *Modern Magnetooptics and Magnetooptical Materials* (Institute of Physics Publishing, 1997).
14. S. Wittekoek, T. J. A. Popma, J. M. Robertson, and P. F. Bongers, "Magneto-optic spectra and the dielectric tensor elements of bismuth-substituted iron garnets at photon energies between 2.2-5.2 eV," Phys. Rev. B **12**, 2777–2788 (1975).
15. F. Hansteen, L. Egil Helseth, T. H. Johansen, O. Hunderi, A. Kirilyuk, and T. Rasing, "Optical and magnetooptical properties of bismuth and gallium substituted iron garnet films," Thin Solid Films **455–456**, 429–432 (2004).
16. V. Doormann, J.-P. Krumme, and H. Lenz, "Optical and magneto-optical tensor spectra of bismuth-substituted yttrium-iron-garnet films," J. Appl. Phys. **68**, 3544–3553 (1990).
17. K. P. Belov, A. K. Zvezdin, A. M. Kadomtseva, and R. Z. Levitin, *Orientational Transitions in Rare Earth Magnets* [in Russian] (Nauka, 1979).
18. P. Roschmann and P. Hansen, "Molecular field coefficients and cation distribution of substituted yttrium iron garnets," J. Appl. Phys. **52**, 6257–6269 (1981).

19. T. Okuda, T. Katayama, K. Satoh, T. Oikawa, H. Yamamoto, and N. Koshizuka, "New magneto-optical garnet $Bi_3Fe_5O_{12}$," in *Proceedings of the Fifth Symposium on Magnetism and Magnetic Materials "Recent Advances in Magnetism and Magnetic Materials,"* H. L. Huang and P. C. Kuo, eds. pp. 61–76 (1989).
20. V. I. Burkov, D. E. Balabanov, V. A. Kotov, and G. S. Semin, "Uniaxial magnetic anisotropy and magnetic circular dichroism spectra of ultrathin films of iron garnets" [in Russian], Tech. Phys. **56**, 2073–2075 (1986).
21. B. Vertruyen, R. Cloots, J. S. Abell, T. J. Jackson, R. C. da Silva, E. Popova, and N. Keller, "Curie temperature, exchange integrals, and magneto-optical properties in off-stoichiometric bismuth iron garnet epitaxial films," Phys. Rev. B **78**, 094429 (2008).
22. J.-P. Krumme, V. Doormann, B. Strocka, and P. Willich, "Selected-area sputter epitaxy of iron-garnet films," J. Appl. Phys. **60**, 2065–2068 (1986).
23. G. A. Tyuliev, A. K. Chernazhova, and V. I. Shapovalov, "Change of X-ray photoelectron spectra of iron garnet films by ion bombardment" [in Russian], Phys. Solid State **31**, 117–121 (1989).
24. V. N. Berzhansky, A. N. Shaposhnikov, A. V. Karavainikov, A. R. Prokopov, T. V. Mikhailova, N. F. Kharchenko, I. N. Likienko, Y. N. Kharchenko, O. V. Miloslavskaya, V. A. Kotov, and V. I. Belotelov, "The effect of Faraday rotation enhancement in nanolayered structures of Bi-substituted iron garnets," Solid State Phenomena **200**, 233–238 (2013).